

INVESTIGATION ON DRAG COEFFICIENT OF SUPERCRITICAL WATER CROSS-FLOW PAST CYLINDER BIOMASS PARTICLE AT LOW REYNOLDS NUMBER

by

Zhen-Qun WU, Hui JIN^{*}, Yi-Fei REN, and Lie-Jin GUO

State Key Laboratory of Multiphase Flow in Power Engineering,
Xi'an Jiaotong University, Xi'an, Shaanxi, China

Original scientific paper
<https://doi.org/10.2298/TSCI170804250W>

The supercritical water gasification of biomass technology is a promising approach for the efficient and clean conversion of wet-biomass to hydrogen-rich gas production. Many of the biomass materials are of rodlike shape and gasified in supercritical water fluidized bed. So the particle-fluid two-phase flow behaviors inside supercritical water fluidized bed are of great importance. Constrained by the extreme operating condition, numerical methods, such as the Euler-Euler method and Euler-Lagrange method, are used to study the flow behaviors inside the supercritical water fluidized bed. As the accuracy of these methods are depended on the drag force model and there is little investigation on that at supercritical condition, this work is focused on the drag coefficient of cylinder biomass particle with different ratio of length to diameter. The simulated results show that there is no difference for the drag coefficient of a certain particle at different condition when the Reynolds number is same. The variation tendency of the pressure and viscous drag coefficient with Reynolds number and the ratio of length to diameter is also given in this paper.

Key words: *cylinder biomass particle, drag coefficient, supercritical water, numerical simulation*

Introduction

Biomass has been a major source of energy for a long history, and it is considered as a renewable and abundant energy resource [1, 2]. In recent years, the supercritical water (SCW) gasification of biomass technology has attracted extensive attention as it can avoid the energy intensive drying step and convert biomass to hydrogen-rich gas products efficiently and cleanly [3-6]. The supercritical fluidized bed is a promising reactor which can solve the plugging problem resulted from the formation of char during the gasification process. For the efficient reactor design, scaling up and operating condition optimization, it is necessary to study the detail of the particle-fluid flow behaviors inside the supercritical water fluidized bed [7]. The CFD provides a convenient method without the limitation by experimental method at high temperature and pressure.

* Corresponding author, e-mail: jinhui@mail.xjtu.edu.cn

For the simulated study of granular flow, there are two approaches, the Euler-Euler method and Euler-Lagrange method, and the accuracy of them has a great dependence on the drag force model. In general, many of the biomass resources are of rodlike shape, especially the cylinder shape, such as the straws [8]. Besides, compressing the biomass resources into cylinder particle is a usual way of utilization. As the particle shape have a great influence on the flow field, the investigation on the SCW flow past cylinder biomass particle is significant. Now, extensive experimental and numerical studies have been done focusing on the fluid-flow past a cylinder at ambient condition. Zdravkovich [9] has compiled almost all the experimental, analytical and numerical results of flow past cylinders and divided the phenomenon into five flow regimes based on the Reynolds number. Batchelor [10] has derived an approximate drag expression of cylinder with the symmetry axis parallel and perpendicular to the stream-wise, which is validated for slender cylinder only. Rajani *et al.* [11] did a numerical study of 2-D and 3-D flow past a cylinder in different laminar flow regimes.

However, the study of the flow past cylinder at supercritical condition has been little so far. So in this paper, a numerical 3-D simulated work was conducted to study SCW flow past a finite cylinder particle for Reynolds number of 10 to 150. The effect of the ratio of length to diameter was also taken into account.

Numerical formulation

As the heat transfer was not taken into consideration, the transport properties were regarded as constant. A laminar incompressible flow model was used:

$$\vec{u} = 0 \tag{1}$$

$$\rho \frac{\partial \vec{u}}{\partial t} = \rho(\vec{u} \cdot \nabla) \vec{u} - \nabla p + \mu \nabla^2 \vec{u} \tag{2}$$

when in the steady flow model, the first term of eq. (2) was neglected. Where \vec{u} is the velocity, ρ – the density, p – the pressure, and μ – the viscosity. The drag force F_d and drag coefficient C_d were calculated:

$$F_d = \mu \int_S \vec{u} \cdot \vec{n} dS - \int_S p \vec{i} \cdot \vec{n} dS = F_{dv} + F_{dp} \tag{3}$$

$$C_d = \frac{F_d}{\frac{1}{2} \rho u^2 DL} = C_{dv} + C_{dp} \tag{4}$$

where D and L are the diameter and length of the cylinder particle, respectively, \vec{n} – the unit normal vector of particle surface, and \vec{i} – the unit vector of stream-wise. The F_{dv} and F_{dp} are viscous and pressure drag force, and the C_{dv} and C_{dp} are viscous and pressure drag force coefficient.

Numerical consideration

From the flow regime divisions by Zdravkovich [9], it can be seen that, for a infinite cylinder, the laminar flow regime with periodic vortex shedding is included in the investigated Reynolds number range. A fully computational domain was adopted and a quarter of it was shown in fig. 1. To avoid the boundary blockage effect, the size of the domain was chosen as $40D \times 20D \times 20D$ corresponded to the X-, Y-, and Z-axes, when the diameter and length both equal to D . As the length was variable in this work, the size of the flow domain would be adjusted in the direction of the length of the particle, to keep the distance from particle surface to flow domain boundary constant.

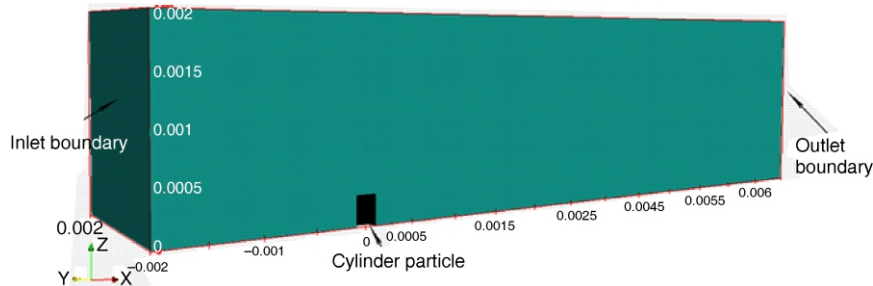


Figure 1. Schematic diagram of quarter of the flow domain

The particle center was located in the center of the Y- and Z-direction with $10D$ to the left patch and the symmetry axis of cylinder particle was corresponding to the Z-direction. For the velocity boundary condition, the left patch was set as inlet boundary with fixed uniform inflow velocity and the right patch was set as outlet boundary with a zero gradient. The particle surface was set as no-slip boundary and the other patches were set as slip boundary. For the pressure boundary condition, except the right patch with a fixed pressure value, the others were all set with a zero gradient.

The mesh was generated by SnappyHexMesh, a mesh generation utility of OpenFOAM. As large gradient occurred near the particle surface, the mesh at this region need to be refined. Through SnappyHexMesh, the resolution of the mesh was controlled by the size of the background mesh and the refinement level of the geometry surface. In this work, the background mesh size was set as $10/D$. For the mesh independence validation, a cylinder particle with the ratio of height to diameter (L/D) of 3 and three kinds of refinement level, 3-5, were used. The operating condition was 0.1 MPa and 300 K for Reynolds number of 30. From the simulated results shown in tab. 1, it can be gotten that the refinement level of 4 was fine enough.

Table 1. Results of mesh independence validation

Refinement level	3	4	5
Mesh number	874360	1567928	4258565
C_d	1.917	1.915	1.915

Simulated results

Numerical method validation

Now, numerous researches have been done for the study of the drag coefficient of non-spherical particle. In this work, simulation about particle with different sphericity at 0.1 MPa and 300 K was conducted firstly and the simulated results were compared to the published data in [12] as shown in fig. 2. The Reynolds number was defined as $\rho u D / \mu$. The D used in [12] was the equivalent volume spherical diameter, while in this paper it was the cylinder diameter. As a result, in this comparison, the Reynolds number corresponding the data in literature was transformed to that based on the

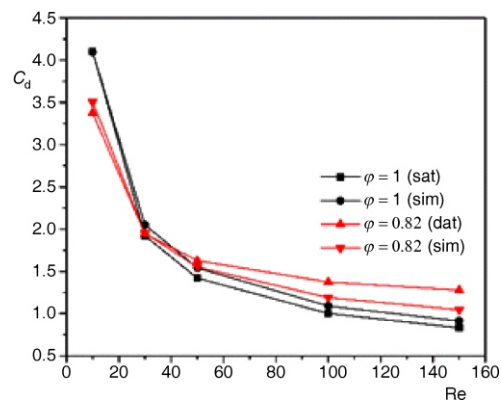


Figure 2. Comparison of simulated drag coefficient to that published data

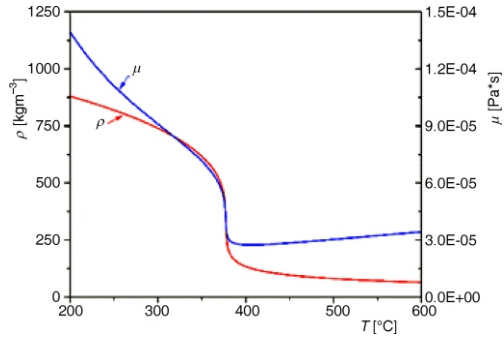


Figure 3. The change of the water dynamic properties near the critical point

Table 2. Drag coefficient at different conditions when $L/D = 3$

Re	10	30	50	100	150
23 MPa, 633.15 K	3.310	1.882	1.509	1.171	1.038
23 MPa, 663.15 K	3.309	1.882	1.508	1.171	1.039
23 MPa, 873.15 K	3.310	1.881	1.508	1.171	1.038
0.1 MPa, 300 K	3.309	1.882	1.508	1.169	1.036

Table 3. Viscous and pressure drag coefficients at different condition when $L/D = 3$

Re		10	30	50	100	150
23 MPa, 633.15 K	C_{dv}	1.672	0.821	0.595	0.389	0.306
	C_{dp}	1.638	1.061	0.914	0.782	0.732
23 MPa, 663.15 K	C_{dv}	1.672	0.821	0.595	0.389	0.306
	C_{dp}	1.637	1.061	0.913	0.782	0.732
23 MPa, 873.15 K	C_{dv}	1.672	0.821	0.595	0.389	0.306
	C_{dp}	1.637	1.060	0.913	0.782	0.732
0.1 MPa, 300 K	C_{dv}	1.672	0.821	0.595	0.387	0.305
	C_{dp}	1.638	1.061	0.913	0.781	0.731

cylinder diameter. From fig. 2, it can be seen a good consistence between the simulated results and the published data. So the numerical method used in this work has good accuracy and reliability.

Drag coefficient of cylinder particle at subcritical and supercritical condition

The SCW has unique dynamical properties, which is a fluid medium different from both the liquid and gas. When the operating condition is near the critical point, as can be seen in fig. 3, the properties of water change dramatically with temperature. In tab. 2, it was displayed that the simulated drag coefficients of water flow past a cylinder particle for different Reynolds number at subcritical and supercritical condition with the ratio of height to diameter of 3. It was also made a comparison to that at ambient condition. The comparing result shows that there is little difference for the same Reynolds number at different operating conditions.

For the further comparison, the viscous and pressure drag coefficients were also given in tab. 3. The values also show a good consistence at different operating conditions when the Reynolds number is same. As shown in eqs. (3) and (4), the viscous and pressure drag coefficients have a great dependence on the flow field distribution. From previous, conclusions can be obtained that for the same Reynolds number, the hydrodynamics of water flow past a cylinder particle at supercritical condition is same with that at ambient condition.

Drag coefficient of cylinder particle with different ratio of height to diameter

The ratio of height to diameter is a main shape factor of cylinder particle, which can influence the flow characteristics greatly. In this work, five kinds of cylinder particles with different values of $L/D = 1, 3, 5, 8, 10$, were investigated at supercritical condition, 23 MPa and 873.15 K. The simulated results of drag coefficient were shown in fig. 4. In fig. 4(a), it can be observed that the influence of the particle shape on drag coefficient get weakened with the increment of L/D . When the value L/D is greater than 3, the drag coefficients of different particle are close at same Reynolds number. At different Reynolds number, the particle shape also has different influence on drag coefficients. When at the low Reynolds number, the drag coefficients of different particle has big deviation, and with the increment of Reynolds number, the deviation get less. From figs. 4(a) and 4(b), it can be observed that, when Reynolds number is 10, the parti-

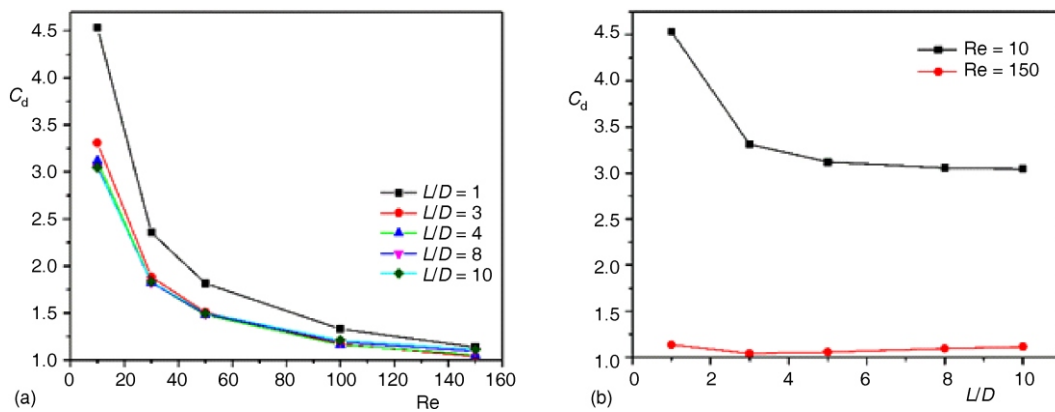


Figure 4. (a) Drag coefficient of cylinder particle to Re with different value of L/D , (b) to L/D at Re of 10 and 150

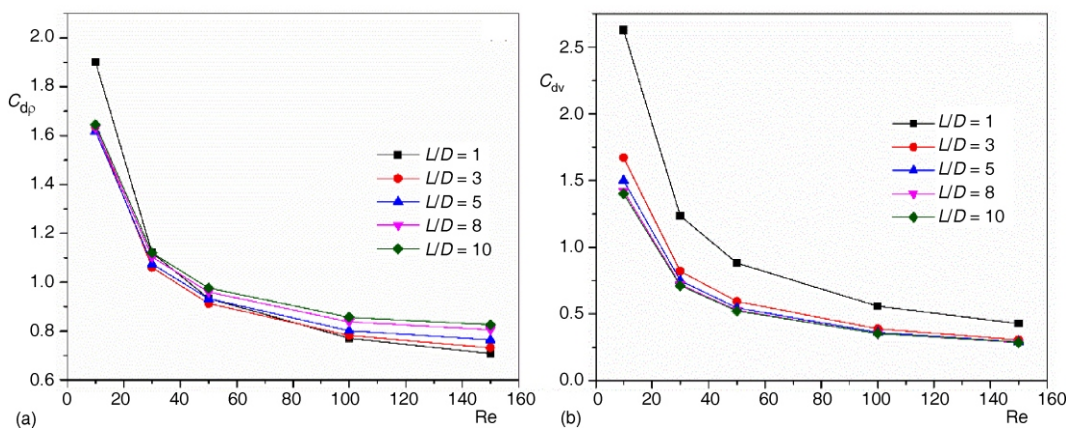


Figure 5. (a) The pressure drag coefficient, (b) the viscous drag coefficient

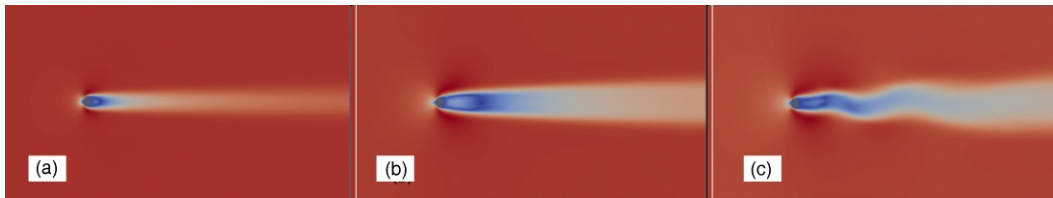


Figure 6. Flow field at the center cross plan of the cylinder at $Re=100$; (a) $L/D=1$, (b) $L/D=5$, (c) $L/D=10$

cle with larger L/D has a larger drag coefficient, and when Reynolds number is 150, the drag coefficient decreases with L/D firstly and then increases. This is because of that, with the increment of L/D , the shape character of cylinder particle approaches that of infinite cylinder. From the flow regime division in [9], the flow regime of infinite cylinder is laminar flow with periodic vortex shedding. The pressure and viscous drag coefficient are also given in fig. 5 for a further analysis.

As can be seen in figs. 5(a) and 5(b), when the value of L/D is 1, the shape character has a great influence on the pressure and viscous drag coefficient, which is consistent with the total drag coefficient shown in fig. 4(a). In fig. 5(a), when the value of L/D is greater than 3, the pressure drag coefficients are close at low Reynolds number. As can be seen in fig. 6, the particle with a larger value of L/D has a wake zone with more violent vortex and reaches the vortex shedding flow regime sooner. For the wake zone with vortex has a lower pressure, the particle with a larger value of L/D has a larger pressure drag coefficient when the Reynolds number is 150. For the viscous drag coefficient, from fig. 5(b), it can be seen that the value of L/D has a big influence on the viscous drag coefficient at low Reynolds number. When the value of L/D is greater than 3, the viscous drag coefficients are almost same at Reynolds number of 150. With the cooperation of pressure and viscous drag coefficient, the total drag coefficient shows the special varied tendency with the Reynolds number and value of L/D .

Conclusion

In this paper, numerical study was conducted to the drag coefficient of SCW cross-flow past the finite cylinder biomass particle at low Reynolds number. Considering the flow regime corresponding the study Reynolds number range, a laminar incompressible flow model and a full computational flow domain were used in this work. From the simulated results, it can be concluded that:

There is no difference for the drag coefficient, including the viscous and pressure drag coefficient, of certain cylinder particle between at ambient condition and at subcritical and supercritical condition.

The influence of shape character on the coefficient get weakens, with the increment of the ratio of length to diameter. In the range of Reynolds number from 10 to 150, for the pressure drag coefficient, the shape character has a larger influence at high Reynolds number. On the contrary, for the viscous drag coefficient, the influence is larger at low Reynolds number.

Acknowledgment

This work was financially supported by the National Key R&D Program of China (Contract no. 2016YFB0600100), the National Natural Science Foundation of China (Contracts No. 51776169 and 51323011)

Nomenclature

C_d	– drag coefficient
C_{dp}	– pressure drag coefficient
C_{dv}	– viscous drag coefficient
D	– cylinder diameter, [m]
F_d	– drag force, [N]
F_{dp}	– pressure drag force, [N]
F_{dv}	– viscous drag force, [N]
\vec{i}	– unit vector in X direction
L	– cylinder length, [m]
\vec{n}	– unit normal vector of surface
p	– pressure, [Pa]
Re	– Reynolds number ($=\rho u D/\mu$)
S	– surface area, [m ²]
\vec{u}	– velocity, [ms ⁻¹]
u	– module of velocity, [ms ⁻¹]

Greek symbols

ρ	– density, [kgs ⁻³]
μ	– viscosity, [m ² s ⁻¹]

Subscripts

d	– drag
p	– pressure
v	– viscous

Acronym

SCW	– supercritical water
-----	-----------------------

References

- [1] Zhao, X., *et al.*, Biomass-Based Chemical Looping Technologies: the Good, the Bad and the Future, *Energy & Environmental Science*, 10 (2017), 9, pp. 1885-1910
- [2] Jin, H., *et al.*, Supercritical Water Synthesis of Nano-Particle Catalyst on TiO₂ and its Application in Supercritical Water Gasification of Biomass, *Journal of Experimental Nanoscience*, 12 (2016), 1, pp. 1-11
- [3] Cao, C., *et al.*, High-Efficiency Gasification of Wheat Straw Black Liquor in Supercritical Water at High Temperatures for Hydrogen Production, *Energy & Fuels*, 31 (2017), 4, pp. 3970-3978
- [4] Jin, H., *et al.*, Supercritical Water Synthesis of Bimetallic Catalyst and Its Application in Hydrogen Production by Furfural Gasification in Supercritical Water, *International Journal of Hydrogen Energy*, 42 (2017), 8, pp. 4943-4950
- [5] Jin, H., *et al.*, Experimental Investigation on Methanation Reaction Based on Coal Gasification in Supercritical Water, *International Journal of Hydrogen Energy*, 42 (2017), 7, pp. 4636-4641
- [6] Cao, W., *et al.*, Hydrogen Production from Supercritical Water Gasification of Chicken Manure, *International Journal of Hydrogen Energy*, 41 (2016), 48, pp. 22722-22731
- [7] Su, X., *et al.*, Numerical Study on Biomass Model Compound Gasification in a Supercritical Water Fluidized Bed Reactor, *Chemical Engineering Science*, 134 (2015), Sep., pp. 737-745
- [8] Nan, W., *et al.*, Numerical Analysis on the Fluidization Dynamics of Rodlike Particles, *Advanced Powder Technology*, 27 (2016), 5, pp. 2265-2276
- [9] Zdravkovich, M. M., Flow around Circular Cylinders – Vol. 1: Fundamentals, Oxford Science Publications, Oxford, UK, 1997
- [10] Batchelor, G. K., Slender-Body Theory for Particles of Arbitrary Cross-Section in Stokes Flow, *Journal of Fluid Mechanics*, 44 (2006), 3, pp. 419-440
- [11] Rajani, B. N., *et al.*, Numerical Simulation of Laminar Flow Past a Circular Cylinder, *Applied Mathematical Modelling*, 33 (2009), 3, pp. 1228-1247
- [12] Yow, H. N., *et al.*, Drag Correlations for Particles of regular shape, *Advanced Powder Technology*, 16 (2005), 4, pp. 363-372